Available online at www.sciencedirect.com
ScienceDirect
Catalysis Today 128 (2007) 245–250
CATALYSIS TODAY
www.elsevier.com/locate/cattod

EXAFS study and photocatalytic properties of un-doped and iron-doped ZrO_2-TiO_2 (photo-) catalysts

M.C. Hidalgo [a], G. Colón [a], J.A. Navio [a,*], M. Macias [a], V.V. Kriventsov [b], D.I. Kochubey [b], M.V. Tsodikov [c]

[a] *Instituto de Ciencia de Materiales de Sevilla, Centro Mixto CSIC-Universidad de Sevilla and Dpto. de Química Inorgánica, Universidad de Sevilla, Spain*
[b] *Boreskov Institute of Catalysis, SB RAS, Lavrentyev prosp. 5, Novosibirsk 630090, Russia*
[c] *A.V. Topchiev Institute of Petrochemical Synthesis, 29 Leninskii prosp., Moscow 117912, Russia*

Available online 21 August 2007

Abstract

The local zirconium and iron arrangements of the iron-doped ZrO_2-TiO_2 system, prepared by sol–gel impregnation method, were studied by EXAFS spectroscopy. Only a tetragonal ZrO_2 structure is located on TiO_2 surface. For the iron-doped ZrO_2-TiO_2 system, the presence of the Fe-O-Fe species as well as and Fe-O-Zr species located on the surface/pre-surface region are shown; it seems that iron is heterogeneously distributed, forming small iron oxide nanoclusters and Fe_x/ZrO_2 (tetragonal) spots at the catalyst surface. The photocatalytic activity of the un-doped and iron-doped binary system ZrO_2-TiO_2 was investigated in two kind of photoreactions: the salicylic acid photooxidation and the photocatalytic reduction of Cr(VI). Different photocatalytic behaviour has been found for the un-doped and iron-doped ZrO_2-TiO_2 systems which have been explained in terms of the EXAFS study.

This study represents an example of attempt to prepare a new potential photoactive mixed oxide system, containing two ions (Ti^{4+} and Zr^{4+}) with good photocatalytic activity if it is compared with commercial TiO_2 (Degusssa P25) calcined at 600 °C.

Keywords: EXAFS; Heterogeneous photocatalysis; Surface; Sol–gel; Iron-doped; ZrO_2; TiO_2

1. Introduction

Illumination of semiconductor particles suspended in water to catalyse oxidative or reductive processes of substrates present in solution is a well-known process named heterogeneous photo-catalysis, especially useful for transformation of toxic substances into less harmful products [1,2]. Although TiO_2 is the most commonly used photo-catalyst, attention has been paid in recent years to metal-doped titania samples (testing efficiency) to replace the bare TiO_2. Results have been controversial, depending on multiple factors such as nature of dopant, metal loading, preparation method, calcination temperature, etc. [3]. Generally, no direct correlation between UV–vis spectroscopic features and photochemical activity could be found, and the preparation method seems to be one of the most important factors for the reactivity of the catalyst.

In previous papers [4,5] polycrystalline zirconium titanate, $ZrTiO_4$, was investigated as a potential photocatalyst. TiO_2 and ZrO_2 are both n-type semiconductors and recently the photocatalytic properties of the binary system ZrO_2-TiO_2 has been reported [6–8].

Concerning the iron-doped commercial TiO_2 (Degussa P25), it was shown [9] that although wet impregnation method does not seem to be a suitable procedure to obtain a uniform distribution of the dopant into the matrix, the use of $Fe(acac)_3$ instead of $Fe(NO_3)_3$ yields a more homogeneous distribution of iron at the surface.

Structural study of the iron location at the surface seems to be a crucial step for understanding correlation between the iron content and the preparation method with the catalytic activity of samples. Similar studies have been recently carried out using Fe/ZrO_2. Thus, in paper [10], the effect of iron doping on ZrO_2

* Corresponding author.
E-mail address: navio@us.es (J.A. Navio).

0920-5861/$ – see front matter © 2007 Elsevier B.V. All rights reserved.
doi:10.1016/j.cattod.2007.07.010

was studied and Fe/ZrO_2 system was tested for several photocatalytic reactions. EXAFS structural studies [11,12] reveal that, for the sol–gel prepared samples, iron seems to form a two-dimensional layer structure that becomes a segregated oxide at higher loading. This segregated iron oxide could be in principle the responsible for the low photocatalytic activity of these systems.

This paper is devoted to a study mainly by EXAFS spectroscopy of un-doped and iron-doped ZrO_2-TiO_2 systems obtained by impregnation procedures from a core highly photoactive TiO_2 (Degussa, P25). The photocatalytic efficiency of the mixed oxides in comparison with that exhibited by the commercial TiO_2, was investigated by two kinds of selected catalytic reactions; on one hand the photocatalytic oxidation of salicylic acid and, on the other, the photocatalytic reduction of Cr(VI). A correlation between structural study and photocatalytic properties is proposed.

2. Experimental

2.1. Preparation of samples

The samples studied were prepared by means of sol–gel impregnation method. The ZrO_2-TiO_2 system was prepared by using $ZrOCl_2{\cdot}8H_2O$ and TiO_2 Degussa P25 as precursors, being the ZrO_2 content of about 10 wt.%. ZrO_2-TiO_2 mixed oxide was obtained by precipitation of $ZrOCl_2{\cdot}8H_2O$ on TiO_2 suspension in bidistilled water at pH 10, and using ammonia as precipitating agent. The gel obtained was filtered and repeatedly washed in order to eliminate Cl^- anions, and finally dried in oven at 110 °C overnight. Iron-doped system was obtained by impregnation technique being the iron loading ca. 1.0 wt.% as Fe_2O_3. Thus iron doping was performed by pouring down the corresponding amount of $Fe(acac)_3$ in ethanol solution. Samples were finally dried at 110 °C overnight and then calcined at 600 °C during 2 h. Those sets of samples were named as impregnation samples prepared with/without iron.

Cr(VI) solution was prepared by using analytical grade $K_2Cr_2O_7$ (Aldrich 99%), being the solution at acid pH of 2. Salicylic acid (Aldrich, >99%) was prepared by dissolving the solid in deionized water.

2.2. EXAFS method

EXAFS spectra of the Ti-K, Zr-K, Fe-K edges for all the samples were obtained at the EXAFS Station of Siberian Synchrotron Radiation Center. The storage ring VEPP-3, with electron beam energy of 2 GeV and an average stored current of 80 mA, has been used as the source of radiation. The X-ray energy was monitored with a channel cut Si(1 1 1) monochromator. The EXAFS spectra of the Ti-K and Zr-K edges were recorded under transmission mode, using two ionization chambers as detectors. The EXAFS spectra of the Fe-K edge were recorded under florescent mode. For the Ti-K edge measurements, a harmonics rejection was performed by using a gold mirror. For transmission EXAFS measurements, the samples were prepared as pellets with thickness varied to obtain a 0.5–1.0 jump at the Ti-K and Zr-K absorption edges. The EXAFS spectra were treated using the standard procedures [13]. The background was removed by extrapolating the pre-edge region onto the EXAFS region in the forms of Victoreen's polynomials. Three cubic splines were used to construct the smooth part of the adsorption coefficient. The inflection point of the edge of the X-ray absorption spectrum was used as initial point ($k = 0$) of the EXAFS spectrum. The radial distribution function (RDF) was calculated from the EXAFS spectra in $k^3\chi(k)$ as the modulus of Fourier transform at the wave number interval 4.0–12.0 $Å^{-1}$. Curve fitting procedure with EXCURV92 [14] code was employed to determine precisely the distances and coordination number intervals after preliminary Fourier filtering using the known XRD data for the bulk zirconium, titanium and iron oxides. Debye–Waller factors are fixed (all the values are equal to 0.005 $Å^2$).

2.3. Additional characterisation

X-ray photoelectron spectroscopy (XPS) was carried out on a Leybold Heraeus LHS-10 spectrometer, working with constant pass energy of 50 eV, and using Al Kα radiation as excitation source. X-ray diffraction (XRD) patterns were obtained with a Siemens D-501 diffractometer using Cu Kα radiation and equipped with a Ni filter and a graphite monochromator. The identification of the different crystalline phases in the spectra was accomplished using the JCPDS database. BET surface area measurements were performed by N_2 adsorption at 77 K using a Micromeritics ASAP 2010 analyzer.

The un-doped samples studied here are the same as some of those already reported in Ref. [7] and that the full standard characterization data (XRD, BET, etc.) are given there.

2.4. Photocatalytic activity studies

Photocatalytic runs (2 h) of salicylic acid oxidation and Cr(VI) reduction over the different catalysts (1 g/l) were performed in a Pyrex immersion well reactor (450 ml) using a medium pressure 400 W Hg lamp supplied by Applied Photophysics, showing main emission line at 365 nm. In the both photocatalytic tests, an oxygen flow was used to produce a homogenous suspension of the catalyst in the solution. Before each photo-experiment, the catalysts were settled in suspension with the reagent mixture for 15 min in the dark. The evolution of the initial concentration (ca. 10^{-4} M for both pollutants) was followed by UV–vis spectrometry through the evolution of its characteristics 290 nm and 348 nm bands for salicylic acid and Cr(VI) respectively, using a filtered aliquot ca. 2 ml of the suspension (Millipore Millex25 0.45 μm membrane filter).

3. Results and discussion

3.1. EXAFS study

First of all, it should be mentioned that the curves of radial distribution of atoms (RDA), not presented in this paper, for the

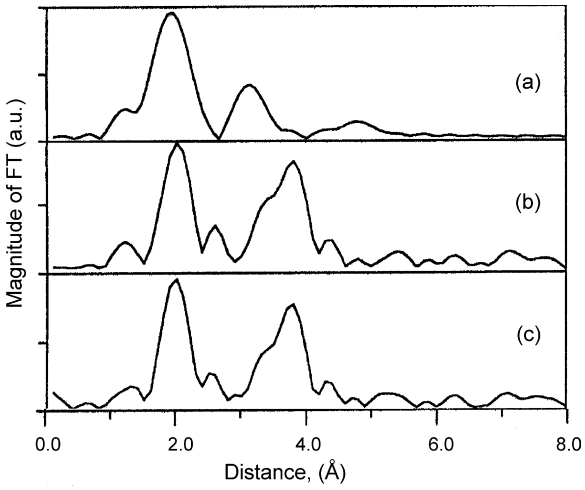

Fig. 1. Radial distribution curves of atoms (RDA) for (a) iron local arrangement of iron-doped ZrO_2-TiO_2 sample and zirconium local arrangement of: (b) undoped ZrO_2-TiO_2 and (c) iron-doped ZrO_2-TiO_2.

local titanium arrangement of all samples studied are similar to that of commercial TiO_2 (Degussa P25). RDA curves of the iron local arrangement of the iron-doped sample prepared by the impregnation method is shown in Fig. 1(a). RDA curves of the local zirconium arrangement for the samples studied are shown in Fig. 1(b and c). EXAFS data (the interatomic distances and coordination numbers) of the studied samples for the iron and zirconium local arrangements are presented in Tables 1 and 2, respectively.

As seen from Table 1, we may assume three structural models describing the iron local arrangement for the doped impregnation samples, which assume different iron localisation [15]. For the trigonal α-Fe_2O_3, the XRD data show two Fe–O distances (1.941, 2.118 Å) and four Fe–Fe distances (2.895, 2.969, 3.61, 3.701 Å). All the models presented yield very

Table 1
EXAFS data (distances, coordination numbers) for iron local arrangement (in assumption of few structural models) of studied samples and known literature data [15] for α-Fe_2O_3

Preparation method	Model number	Bond type	Distance (Å)	Coordination number	*R*-factor (%)
Impregnation with Fe	1	Fe–O	1.97	4.3	23.9
		Fe–Fe	2.86	1.1	
		Fe–Ti	3.04	1.6	
	2	Fe–O	1.98	4.4	22.5
		Fe–Fe	2.88	1.5	
		Fe–Fe	3.04	1.6	
	3	Fe–O	1.98	4.4	22.0
		Fe–Fe	2.93	1.3	
		Fe–Zr	3.29	0.9	
α-Fe_2O_3		Fe–O	1.941, 2.118	3.0, 3.0	
		Fe–Fe	2.895, 2.969	1.0, 3.0	
		Fe–Fe	3.361, 3.701	3.0, 6.0	

Table 2
EXAFS data (distances, coordination numbers) for zirconium local arrangement (in assumption of few structural models) of studied samples and known literature data [16] for $ZrTiO_4$

Preparation method	Model number	Bond type	Distance (Å)	Coordination number	*R*-factor (%)
Impregnation without Fe	1	Zr–O	2.12, 2.31	4.0, 2.3	21.6
		Zr–Zr	3.57, 3.66	1.1, 2.2	
Impregnation with Fe	1	Zr–O	2.10, 2.30	3.9, 2.2	22.7
		Zr–Zr	3.55, 3.62	0.8, 2.1	
$ZrTiO_4$[a]		Zr–O	1.937, 1.948, 2.228	2.0, 2.0, 2.0	
		Zr–Zr	3.328, 3.522, 3.632	2.0, 4.0, 4.0	
		Zr–Ti	3.328, 3.522, 3.632	2.0, 4.0, 4.0	

[a] Debye–Waller factors are fixed (all the values are equal to 0.005 Å).

similar results for the samples; the first Fe–O distances of ca. 1.97–1.98 Å and the second Fe–Fe of ca. 2.86–2.93 Å. The corresponding coordination numbers varied within ca. 4.3–4.4 and ca. 1.1–1.6, respectively. Analysis of the obtained set of distances evidenced the presence of the Fe–O–Fe species seemingly as small iron oxide nanoclusters or layered structures located onto the surface and pre-surface region of the modified titania, ZrO_2-TiO_2 interface or ZrO_2.

The EXAFS data (Table 1) allows the possibility that an additional iron disposition located on the surface/pre-surface region could be formed. Thus, Fe-O-Ti and Fe-O-Zr species might be also considered. It should be noted that, for this prepared impregnation sample, the best assumption is model 3, which corresponds to Fe adsorbed on ZrO_2, probably located on the external surface of the ZrO_2 nanoparticles as has been reported by us [12].

By the analysis of the local Zr arrangement of the impregnation samples, obtained from the RDA curves (Fig. 1(b and c)) and EXAFS data (Table 2), one may assume the formation of mainly tetragonal ZrO_2 phase located on TiO_2 surface. The presence only of Zr–O distances about 2.10–2.31 Å and long Zr–Zr distances of about 3.55–3.66 Å, which are typical for tetragonal ZrO_2 structure, clearly proves this suggestion. In our previous paper [11], a detailed discussion is presented about monoclinic/tetragonal zirconia determination by EXAFS data. Therefore, it seems that iron doping does not influence on the formed structures because the shapes of RDA curves as well as fitting results are similar for both samples. Thus, our conclusion about ZrO_2 structures formed on the TiO_2 surface is in good agreement with the above mentioned hypothesis about iron localisation mainly on ZrO_2 surface. In fact, XPS analysis of the ZrO_2-TiO_2 sample showed a value of ca. 12 wt.% ZrO_2 which is very close to the nominal value of ZrO_2 for the prepared sample. At the same time, XRD study of these binary systems, showed diffraction peaks assigned to TiO_2 (anatase and rutile), and ZrO_2 (tetragonal). All these results clearly indicate that from the preparation procedure reported here, the formation of solid solution is not expected.

Table 3
Photonic efficiency (%) for salicylic acid photooxidation and Cr(VI) photoreduction reactions over un-doped (reference [7]) and iron-doped ZrO_2-TiO_2 systems and for TiO_2 catalyst calcined at 600 °C for 2 h

Catalysts	Salicylic acid	Cr(VI)
TiO_2 (Degussa P25)	14.1	2.8
ZrO_2-TiO_2	15.8	7.0
Fe/ZrO_2-TiO_2	<1	<1

On the other hand, impregnation method should lead to the incorporation of Fe^{3+} heterogeneously distributed only at surface level, and as above discussed it would form small iron oxide nanoclusters or Fe_x/ZrO_2(tetragonal).

3.2. Photocatalytic activity

The photocatalytic activity of the binary system ZrO_2-TiO_2 and TiO_2 calcined at 600 °C for 2 h was tested for salicylic acid photooxidation and Cr(VI) photoreduction. Photonic efficiencies (%) have been calculated by using the following reported expression [17]:

$$\xi = \left[-\frac{(dC/dt)}{P_0} \right] \times 100$$

where dC/dt is the rate of substrate elimination assuming zero order kinetics and P_0 is the photon flux of the lamp (in our case has a value of 2.6×10^{-7} Einstein l^{-1} s^{-1} measured by the chemist actinometer Aberchrome 540); $-(dC/dt)$ was calculated from the slope of the conversion curves at the first stage of the reaction (up to 30 min). In Table 3, the values of the photon efficiencies for the un-doped and iron-doped binary system ZrO_2-TiO_2 as well as for TiO_2 (Degussa P25) used in the studied photoreactions are summarized. Regarding the photoactivity it should be noted that ZrO_2-TiO_2 exhibits slight higher photoefficiences values with respect to TiO_2 calcined at 600 °C for both reactions, having both systems similar surface areas, S_{BET} ~50 m^2/g. However, it is clear from Table 3 that incorporation of Fe^{3+} species on the binary system ZrO_2-TiO_2 results detrimental for the photocatalytic activity in both cases, salicylic acid photooxidation and photoreduction of Cr(VI).

The preparation and photocatalytic properties of Zr^{4+}-doped TiO_2 nanocrystals have been recently reported [8]. It was shown that when the Zr^{4+} content was 6 mol%, the photocatalytic efficiency of $Ti_{0.94}Zr_{0.06}O_2$ was 1.5 times higher than that of pure TiO_2. However, for this kind of system, prepared by sol–gel method, the doping species Zr^{4+} was incorporated into the TiO_2 lattice leading to larger lattice deformation and forming capture traps, which contribute to the higher separation efficiency of the photogenerated carriers.

According with EXAFS results, our prepared ZrO_2-TiO_2 system could be regarded as composite powders of crystalline TiO_2 (anatase and rutile), as inner core, partly covered with in situ precipitated amorphous ZrO_2 which further crystallises as tetragonal ZrO_2 spots upon calcination, as it is schematically showed in Fig. 2. Taking into account that ZrO_2 incorporation does not lead to a solid solution, the observed photoefficiencies must be explained in terms of the core-shell model proposed in Fig. 2.

In previous papers [4,5] the photocatalytic properties of a prepared zirconium titanate, $ZrTiO_4$, was investigated and comparison with the parent oxides TiO_2 and ZrO_2 was reported. In that case, the following activity order, independently of the substrate considered, was found: $TiO_2 \gg ZrO_2 > ZrTiO_4$. Thus, titania, especially in the anatase form, is the most active solid. Zirconia is substantially less active than titania, but it can still be considered as a potential photocatalyst [18,19]. The least active solid is $ZrTiO_4$. Since, ZrO_2 absorbs at much shorter wavelengths, it can be proposed that, for a given flux, the smaller amount of photons absorbed by ZrO_2 can generate more efficient electron–hole pairs, which preferentially separate instead of recombining. At the same time, ZrO_2 possesses good adsorptive properties with respect to the reactants, thus favouring reactions on the adsorbed phase and compensating for its lower absorbance in the UV range.

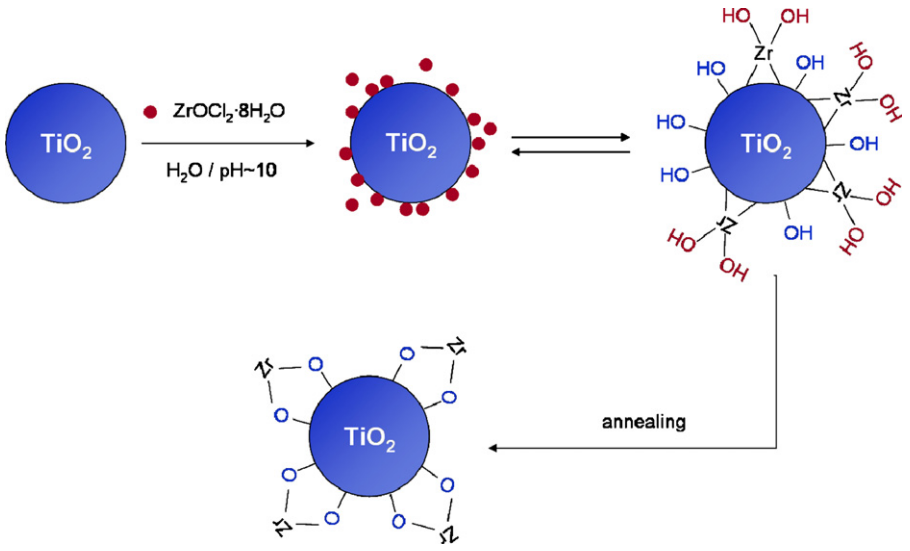

Fig. 2. Synthesis process of the un-doped ZrO_2-TiO_2 and schematic representation of the obtained particles according with EXAFS study.

In the present study we have not tested the photocatalytic activity of a homogeneous system compared with the core-shell binary oxide, ZrO_2-TiO_2; however, to the reported results [4,5] and the present study it seems to be clear that the core-shell ZrO_2-TiO_2 binary system is a good alternative for TiO_2 and consequently for $ZrTiO_4$.

On the other hand, if we assume the model proposed in Fig. 2, the photocatalytic properties of the un-doped binary system ZrO_2-TiO_2 could be explained in terms of the doping metal ions Zr^{4+} onto the catalyst surface. Thus, we propose that the photocatalytic reactions of TiO_2(-Zr) particles take place by the following mechanism:

$$TiO_2 + h\nu \rightarrow e^- + h^+$$

$$Ti^{4+} + e^- \rightarrow Ti^{3+}$$

$$Zr^{4+} + e^- \rightarrow Zr^{3+}$$

$$\rangle OH^- \rightarrow \rangle OH^\bullet$$

$$e^- (\text{or } Ti^{3+}, Zr^{3+}) + O_x \rightarrow O_x{}^-$$

$$h^+ (\text{or } \rangle OH^\bullet) + R_{ed} \rightarrow R_{ed}{}^+$$

where O_x is an electron acceptor and R_{ed} is an electron donor. Thus, on the basis of our results, in this binary system ZrO_2-TiO_2, the dopant Zr^{4+} ions are partially covering the surface, which present a metal loading close to the nominal value. Moreover, ZrO_2 in the bulk is not forming a solid solution, therefore, the charge release and migration in the lattice, suggested by Choi et al. [20] as crucial can be neglected for the charge trapped by Zr^{4+} in the binary system. The Zr^{4+} ions on the surface catalyst would enhance the charge trapping and inhibit the e^-/h^+ pair recombination as a charge separation centre. So, the Zr^{4+} species would enhance the photoactivity by trapping electron that enhance the separation of photogenerated carriers, electrons and holes. The electron trapping at the surface is particularly evident for the enhancement of the rate of Cr(VI) reduction.

According with the photoefficiencies results reported in Table 3, Fe^{3+} ions incorporated at the surface of the ZrO_2-TiO_2 system may be regarded as unfavourable to the good photocatalytic activity exhibited by the un-doped binary ZrO_2-TiO_2 system. The role, of iron dopant in semiconductors based on TiO_2 is controversial [3]. Some authors pointed that Fe^{3+} centres behave as e^-/h^+ recombination centres while some others postulated that its role is to perform the e^-/h^+ separation, enhancing the photocatalytic activity. Accordingly to the detrimental effect of Fe^{3+}-doped ZrO_2-TiO_2 system, the role of Fe^{3+} can be postulated as e^-/h^+ recombination centres blocking the good photocatalytic properties exhibited by the TiO_2(-Zr) system. On the other hand the iron-complexing ability with carboxylic groups is well-known [21]. Thus, it is well-established [22] that carboxylic acid molecules interact with the surface of Fe-TiO_2 catalysts and as a consequence iron atoms are extracted from the catalysts surface as photoactive complexes [Fe-carboxylic acid]$^{n+}$. We did not quantify any dissolved iron species in our photocatalytic runs when the Fe/ZrO_2-TiO_2 system is tested, for which iron species seems to be located on the external surface of the ZrO_2 nanoparticles. Although we have not experimental evidence about the possibly iron species extracted from the surface of the Fe/ZrO_2-TiO_2 system as well as the formation of a photoactive [Fe-salicylic acid]$^{n+}$, however in such a case the photoactivity showed should be expected higher than the detrimental value of the photonic efficiency observed for this kind of photocatalyst (Table 3).

4. Conclusions

The local zirconium and iron arrangements of the iron-doped ZrO_2-TiO_2, prepared by sol–gel impregnation method, were studied by EXAFS spectroscopy. Only a tetragonal ZrO_2 structure is located on TiO_2. For the iron-doped ZrO_2-TiO_2 system, the presence of the Fe-O-Fe species as well as Fe-O-Zr species located on the surface/pre-surface region are shown. On the other hand, it seems that iron is heterogeneously distributed, forming small iron oxide nanoclusters and Fe_x/ZrO_2 (tetragonal) spots at the catalyst surface.

Our study represents an example of attempt to prepare a new potential photoactive mixed oxide system, containing two ions (Ti^{4+} and Zr^{4+}) with good photocatalytic activity if compared with commercial TiO_2 (Degusssa P25) calcined at 600 °C. However, we can conclude that the structural situation of doped system (Zr^{4+} and Fe^{3+}), in the highly photoactive TiO_2, drives its reactivity, and consequently the preparation procedure turns crucial.

Acknowledgements

Authors thanks NATO-Collaborative Research Grant (Ref. EST.CLG.979855), Russian Fund of Fundamental Research (Project N00-03-32407a) and to Spanish ‘‘Ministerio de Educación y Ciencia’’ (Project CTQ2004-05734-C02-02), for partial support for this work. M.C. Hidalgo thanks the Spanish ‘‘Ministerio de Educación y Ciencia’’ (Ramón y Cajal Programme N.2003/1116) for financial support.

References

[1] M. Schiavello (Ed.), ‘‘Heterogeneous Photocatalysis’’, Wiley Series in Photoscience and Photoengineering, vol. 3, J. Wiley and Sons, 1997.
[2] M.R. Hoffmann, S.T. Martin, W. Choi, D.W. Bahnemann, Chem. Rev. 95 (1995) 69.
[3] G. Colón, C. Belver, M. Fernández-García, Nanostructured Oxides in Photocatalysis (Chapter 17), in: M. Fernández-García, J.A. Rodríguez (Eds.), Synthesis, Properties and Application of Oxide Nanomaterials, Wiley, USA, 2007.
[4] H. Courbon, J. Disdier, J.M. Herrmann, P. Pichat, J.A. Navío, Catal. Lett. 20 (1993) 251.
[5] J.A. Navío, G. Colón, J.M. Herrmann, J. Photochem. Photobiol. A: Chem. 108 (1997) 179.
[6] M. Zorn, D. Tompkins, W. Zeltner, M. Anderson, Appl. Catal. B: Environ. 23 (1999) 1.
[7] G. Colón, M.C. Hidalgo, J.A. Navío, Appl. Catal. A: Gen. 231 (2002) 185.
[8] Y.M. Wang, S.W. Liu, M.K. Lü, S.F. Wang, F. Gu, X.Z. Gai, X.P. Cui, J. Pan, J. Mol. Catal. 215 (2004) 137.
[9] (a) J.A. Navío, G. Colón, M.I. Litter, G.N. Bianco, J. Mol. Catal. 106 (1996) 267;

(b) M.I. Litter, J.A. Navío, J. Photochem. Photobiol. A: Chem. 98 (1996) 171.
[10] J.A. Navío, M.C. Hidalgo, G. Colón, S.G. Botta, M.I. Litter, Langmuir 17 (2000) 202.
[11] V.V. Kriventsov, D. Kochubey, J.A. Navío, M.C. Hidalgo, G. Colón, M. Tsodikov, Y. Maksimov, I. Suzdalev, J. Synch. Rad. 8 (2001) 528.
[12] V.V. Kriventsov, D.I. Kochubey, Y.V. Maksimov, I.P. Suzdalev, M.V. Tsodikov, J.A. Navío, M.C. Hidalgo, G. Colón, Nucl. Instr. Meth. Phys. Res. A 470 (2001) 341.
[13] D.I. Kochubey, EXAFS Spectroscopy of Catalysts, Novosibirks, Nauka, 1992.
[14] N. Binsted, J.V. Campbell, S.J. Gurman, P.C. Sthephenson, SERC Daresbury Laboratory EXCURV92 program, 1991.
[15] H.S. Shin, S.J. Kwon, J. Kor. Ceram. Soc. 30 (1993) 499.
[16] R.E. Newnham, J. Am. Ceram. Soc. 50 (1967) 216.
[17] H. Tahiri, N. Serpone, R.L. van Mao, J. Photochem. Photobiol. A: Chem. 93 (1996) 199.
[18] J.M. Herrmann, J. Disdier, P. Pichat, J. Chem. Soc. Faraday Trans. I 77 (1981) 2815.
[19] J.M. Herrmann, J. Disdier, M.N. Mozzanega, H. Courbon, P. Pichat, in: G. Centi, F. Trifiró (Eds.), New Development in Selective Oxidation, Elsevier, Amsterdam, 1990, p. 675.
[20] W. Choi, A. Termin, M.R. Hoffmann, J. Phys. Chem. 98 (1994) 13669.
[21] B.A. Holmen, M.I. Tejedor-Tejedor, W.H. Casey, Langmuir 13 (1997) 2197.
[22] J. Araña, O. González Díaz, J.M. Doña Rodriguez, J.A. Herrera Melián, C. Garriga i Cabo, J. Pérez Peña, M. Carmen Hidalgo, J.A. Navío Santos, J. Mol. Catal. A: Chem. 197 (2003) 157.